# Estuarine forcing of a river plume by river flow and tides

Mark J. Halverson[1] and Rich Pawlowicz[1]

Received 31 March 2008; revised 6 June 2008; accepted 30 June 2008; published 24 September 2008.

[1] Estuarine forcing of a river plume by river discharge and tides is examined with a novel data set capable of characterizing semidiurnal to annual time scales. An instrumented ferry made high-resolution salinity measurements as it crossed the Fraser River plume, British Columbia, Canada, eight times per day over the years 2003–2006. The relative contribution of different forcing factors in controlling the river plume salinity and surface area is examined over the full range of time scales. A Lomb-Scargle periodogram of the plume salinity shows energy concentrated in the semidiurnal and diurnal tidal bands. Diurnal lines contain more energy relative to semidiurnal lines than the respective tidal constituents would suggest. At fortnightly frequencies, local maxima in plume salinity coincide with periods of maxima in daily tidal height, with no phase shift. Thus the estuary adjusts quickly to changes in forcing. The effectiveness of tides in setting the plume salinity is a function of river discharge and is greatest when the river discharge is high and minimal when the river discharge is low. Tidal effects are superimposed onto the long-period river discharge cycle. At time scales of 25 days or longer, the mean river plume salinity decreases quasi-linearly with increasing river discharge, but the change in salinity with river discharge is instantaneous to within the sampling resolution. Plume surface area increases with river discharge, from 200–500 km$^2$ at low river flow to 1000–1500 km$^2$ at high river flow. The magnitude of the surface area is predicted well by scaling the mouth deformation radius.

**Citation:** Halverson, M. J., and R. Pawlowicz (2008), Estuarine forcing of a river plume by river flow and tides, *J. Geophys. Res.*, *113*, C09033, doi:10.1029/2008JC004844.

## 1. Introduction

### 1.1. Estuary-River Plume System

[2] An estuary-river plume system may be broadly decomposed into three interacting components: the estuary, and the near- and far-field plumes [*Hetland*, 2005]. Physically, the estuary and near-field plume are characterized by intense mixing of fresh and salt water. The far-field refers to the region away from the geometric influence of the river mouth, which we would observe as the surface advected river plume. To some degree, these categories also delineate regions dominated by different external forcing factors. Inertial shear mixing dominates in the estuary and near-field and is modulated by variations in river flow and tides, while wind forcing dominates the far-field.

[3] Much of the work on estuaries and river plumes implicitly treats them as separate entities. That is, work on estuaries is principally centered on river and tidal effects within the estuary [e.g., *Hansen and Rattray*, 1965; *Partch and Smith*, 1978; *Geyer and Farmer*, 1989; *Hetland and Geyer*, 2004; *MacCready*, 2007], and work on river plumes is concerned with the effects of, for example, wind stress and ambient flows [e.g., *Chao*, 1988; *Lentz*, 1995a; *Hickey et al.*, 1998; *Fong and Geyer*, 2002; *Hetland*, 2005]. The connection has received little attention since the work of *Garvine* [1975] in the Connecticut River Estuary. Understanding the connection is important because momentum and buoyancy at the mouth will influence river plume dynamics further afield [*Garvine*, 1987], an issue especially important in numerical models of river plumes [e.g., *Hetland*, 2005]. This paper attempts to link the two by identifying the effects of estuarine mixing and advection on basic properties of a river plume.

[4] Tidal and river forcing introduce a wide range of time scales to the problem of estuarine dynamics. Tides operate on semidiurnal, diurnal, and fortnightly time scales, while river forcing typically works on annual time scales. The wide range of time scales is difficult to cover with field studies. Ship-based work cannot capture long time scales without aliasing higher-frequency processes, moorings lack horizontal information, and satellites cannot measure the most important tracer, salinity.

[5] A ferry sampling program in the Strait of Georgia, BC, Canada, has provided a data set capable of identifying the effects of estuary mixing on a river plume over all forcing time scales. The ferry crosses the Fraser River plume, which originates from a strongly forced estuary. Maximum daily tidal range is 5 m, while the river flow varies by a factor of 10 over its annual cycle. The sampling platform, coupled with a strongly forced system, provides a

[1]Department of Earth and Ocean Sciences, University of British Columbia, Vancouver, British Columbia, Canada.


0148-0227/08/2008JC004844$09.00

unique opportunity to study the effects of estuary processes on the properties of a river plume.

### 1.2. Estuarine Mixing and Advection by Tides and River Flow

[6] River flow and tides are the primary external forces that introduce time dependence to estuarine salinity structure. River flow primarily introduces stratification while tides have a tendency to break down stratification. Because the external forcings mix and advect water in an estuary, they should affect basic properties of a river plume.

[7] Tidal asymmetry of estuarine flow favors mixing on ebb tides, when shear is maximized at the interface of the salt wedge and river water. In the Duwamish estuary, *Partch and Smith* [1978] observe that the vertical salt flux is ten times higher during ebbs than floods, and that nearly half of the total vertical salt flux occurs over a relatively short time during the ebb. In the Fraser estuary, *Geyer and Farmer* [1989] observe unstable waves on the salt wedge halocline, and show that the tendency to mix across the interface is a function of the tidal phase. The shear across the interface increases during the ebb phase until the Richardson number reaches a critical value. *Geyer and Farmer* [1989] hypothesize that the estuarine structure should be sensitive to the fortnightly modulation of tidal amplitude because of the sensitivity of shear across the interface to the strength of the ebb tide. Variation of mixing over a spring-neap cycle has been observed in the Columbia [*Jay and Smith*, 1990] and Hudson [*Peters*, 1997] estuaries.

[8] The ability of the tides to drive mixing is a function of river discharge in some estuaries. In the Columbia estuary, river flow modulates the ability of the tides to break down stratification at the salt wedge [*Jay and Smith*, 1990]. During high river flow, stratification is too strong for the largest ebb tides to create enough shear to break down the salt wedge. At low river flow, it is possible for the weakest tides to mix away the salt wedge.

[9] Advection of the estuary salt field by tides has received less attention than mixing, but in anticipation of our results we note that the position of the salt wedge with respect to the river mouth will likely affect plume properties. A salt wedge may move a significant distance over a single tidal cycle [e.g., *Garvine*, 1987; *Kostaschuk and Atwood*, 1990], at times comparable to the length of the salt intrusion itself.

[10] River discharge also sets the position of the salt wedge. An early theoretical investigation by *Hansen and Rattray* [1965] suggested that the steady state length of the salt intrusion should be inversely proportional to river flow. The inverse relation has been observed in number of estuaries [e.g., *Abood*, 1974; *Kostaschuk and Atwood*, 1990; *Jay and Smith*, 1990; *Monismith et al.*, 2002]. A long estuary presents a greater surface area for mixing compared to a short estuary.

[11] With the cumulative understanding of mixing and advection processes in estuaries, we proceed to study their effects on the salinity and surface area of a river plume. As such this paper is organized as follows: In section 2 we describe the Fraser River, estuary, and Strait of Georgia. In section 3 we describe the characteristics of ferry sampling, the satellite imagery, and the forcing records. In section 4 we describe the mean horizontal structure of the plume and analyze the time series of salinity and surface area. In section 5 we interpret the time series in terms of estuarine mixing and advection processes, and compare the results to other systems. Finally, in section 6 we summarize this work.

## 2. Study Area: Strait of Georgia and the Fraser River

[12] The Fraser River empties into the Strait of Georgia (hereafter SoG), a midlatitude semienclosed coastal basin situated between mainland British Columbia and Vancouver Island. The Fraser River is the single largest point source of fresh water into the SoG, making up 50–85% of the total discharge of fresh water [*Waldichuk*, 1957; *Crean et al.*, 1988; *Pawlowicz et al.*, 2007]. Figure 1 shows a map of the lower SoG with 551 nm reflectance measured using the Moderate Resolution Imaging Spectroradiometer (MODIS). The Fraser River plume is formed by discharge from each of its three arms. The southernmost arm, carrying 87% of the total river flow [*Crean et al.*, 1988], is 15 km due south of Vancouver. The SoG is approximately 30 km wide here, and observations show the plume can span the SoG under some conditions [*Tabata*, 1972]. Before reaching the SoG, the river follows a 9 km channel through tidal mud flats ending at the Sand Heads meteorological station. The channel is periodically dredged to a navigable depth of about 10 m but has a few pools of roughly 18 m depth. From the seaward extent of the mud flats the plume is detached from the bottom as the depth of the SoG increases quickly to greater than 100 m.

[13] Direct measurements of the Fraser River discharge at the mouth are not available but necessary for this paper. Thus we form an estimate according the method in Appendix A. The estimated daily average discharge at the mouth is shown in Figure 2 along with the measured discharge at Hope, the gauging station traditionally chosen to represent the river discharge. Discharge values in this paper will always be given for the mouth. Fraser flow is uncontrolled, and the annual discharge cycle is driven by early summer snow melt, providing freshet flows which peak in early June. Flows at the river mouth at this time range from 7500 $m^3\ s^{-1}$ to 9000 $m^3\ s^{-1}$ over 2003–2006, which is 1000–2000 $m^3\ s^{-1}$ higher than the flow at Hope. By late summer, the discharge reduces to 1000–1500 $m^3\ s^{-1}$ and remains low (with the exception of fall 2004) until the following spring. Our estimate shows the discharge at the mouth to be about 500 $m^3\ s^{-1}$ higher than the discharge at Hope during normal winter flows. Winter rain storms often cause the discharge to more than double over the span of a few days, commonly from 1500 $m^3\ s^{-1}$ to 3000 $m^3\ s^{-1}$ or higher during rare cases (e.g., October 2003). During rain storms our correction can exceed 1000 $m^3\ s^{-1}$.

[14] Tides in the SoG are of the mixed type and characteristic of the temperate eastern Pacific. Both spring/neap (i.e., lunar phase) and tropic/equatorial (i.e., lunar declination) cycling produce a sizeable fortnightly modulation, thus we will generically refer to these as the fortnightly cycle. The minimum daily tidal range over the study period was 1.9 m, while the maximum was 5.0 m. Representative along-strait ebb tide currents reach 1 m/s in the narrow southern end of the SoG, near Tsawwassen, and decrease

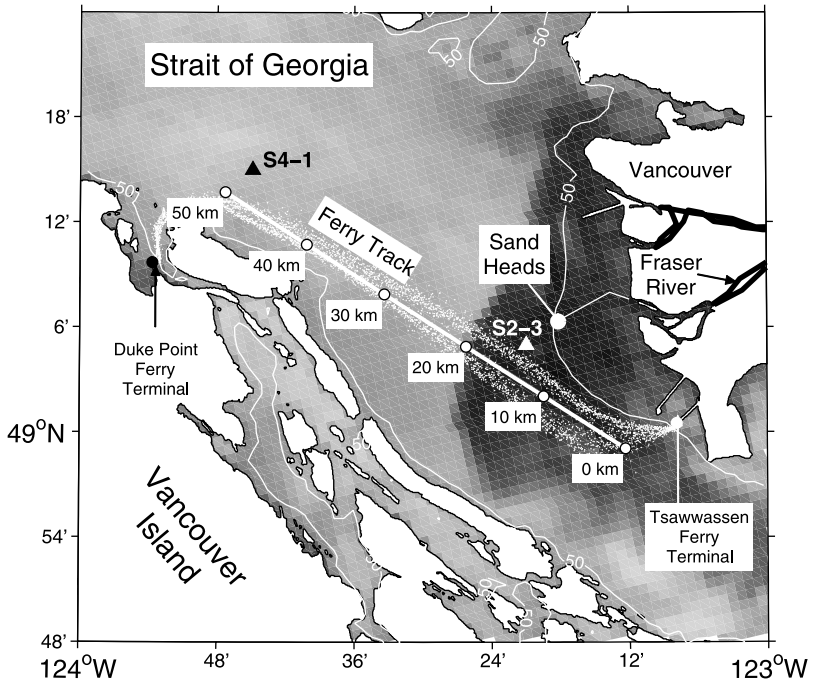


**Figure 1.** Map of the lower Strait of Georgia plotted on a MODIS 551 nm 1 km resolution image. The image was taken on 19 July 2005, while the river discharge was ~6000 $m^3$ $s^{-1}$. The plume appears as dark shades signifying a high reflectance. The small white points are 3 months of subsampled GPS fixes from the ferry. Westbound sailings are north of the eastbound sailings.

northward as the SoG widens [see *Crean et al.*, 1988, Figure 1.19]. In the vicinity of the plume we estimate maximum tidal excursion to be 10 km. Tidal heights used in this paper were those predicted for Point Atkinson, BC, located 25 km north of the Fraser River mouth. Tidal records are available closer to the river mouth, but we sought a time series uncontaminated by the river stage.

## 3. Methods and Data

### 3.1. Ferry Observations

[15] The primary data set was acquired from a collection of sensors aboard the British Columbia Ferry Services Inc. vessel, The Queen of New Westminster. For a month in spring 2003, another instrumented vessel, the Queen of Alberni, serviced this route. The ferry makes four round trips from Tsawwassen to Duke Point each day (see Figure 1). The track essentially runs along strait, oriented to the northwest/southeast. The first sailing departs Tsawwassen at 0515 local time, and the last sailing departs Duke Point at 2345 local time. A complete transect covers 70 km and takes 2 h.

[16] Ferry data began on 13 January 2003, and continued until 29 October 2006. Every winter the ferry was removed for an annual refit, creating month-long data gaps. Occasional instrumentation problems caused additional gaps in the data record, the longest being a month in May 2004.

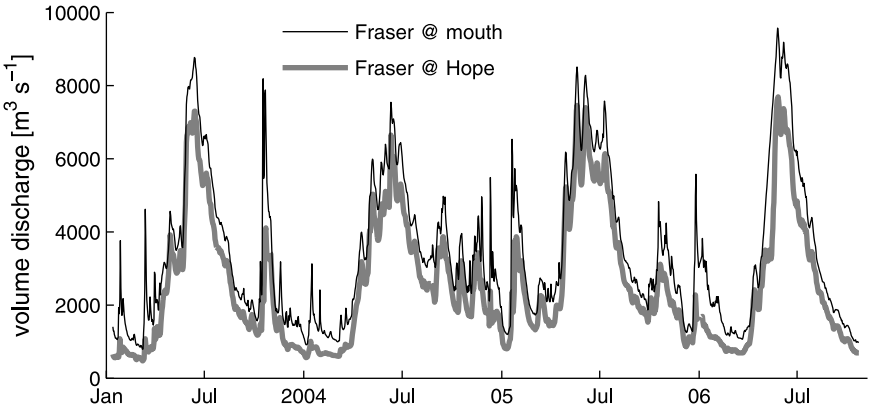


**Figure 2.** A time series of Fraser discharge at two locations, Port Mann (thin black) and Hope (thick gray). The discharge at Port Mann has been estimated according to the method described in Appendix A whereas the Hope discharge is measured directly by the Water Survey of Canada.

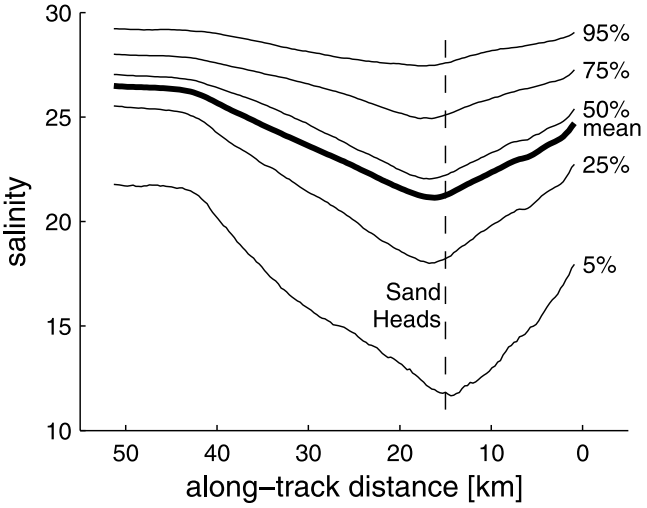


**Figure 3.** Average horizontal plume salinity structure (thick line) with 5, 25, 50, 75, and 95% percentiles (thin lines) as functions of along-strait distance. The vertical dashed line marks the along-strait distance closest to the Fraser River mouth.

Other gaps typically last a few days and occur infrequently and sporadically through the time series.

[17] The instrument suite includes chemistry-free sensors to measure several oceanographic variables. In this paper, we will only make use of salinity, measured by a Seabird SBE45, and GPS position. The thermosalinograph samples at 5 s intervals and GPS fixes were taken at 10 s intervals. The thermosalinograph precision is ±0.005 PSU, but regular lab and factory calibrations revealed that fouling occasionally freshened the salinity by up to 0.6 PSU. Because the plume was identified by relative changes in salinity along a transect, and because the salinity can vary by 10 PSU in a single transect, we do not correct for fouling.

[18] Our system, located in the engine room, draws a continuous stream of water from the ship's engine seawater cooling system. Engine cooling water is pumped into a sea chest, located midship, from a depth of 3.5 m. Hull depth may vary by up to 40 cm depending on payload. A direct comparison of the ferry salinity with CTD profiles taken near the ferry suggest that the source water is effectively drawn from about 2 m because of mixing by the hull.

[19] The ferry travels at roughly 20 knots, and thus the highest achievable spatial resolution is 40 m (for a 5 s sampling interval). However there is a delay of about 3 min between the time water enters the sea chest and the time when it passes through our instruments. While in the sea chest, water can mix and effectively decrease the spatial resolution. If we take 3 min as the minimum temporal resolution, the spatial resolution becomes 1.9 km.

[20] Data quality control and processing includes discarding data obtained while in port and during equipment servicing. The data is binned to 30 s intervals, and then gridded according to along-strait distance by projecting the tracks onto a line running along the center of the SoG (see Figure 1).

[21] The high spatial resolution allows the plume boundaries to be identified from a ferry transect according to the salinity record. The details of how the plume is chosen is outlined in Appendix B. Spatial averages of relevant sections of the ferry track are taken to form time series. We will work with high- and low-resolution time series of plume surface area and salinity. The high-resolution time series are irregularly spaced in time because of the ferry sailing schedule. The low-resolution version is constructed by forming daily means of the high-resolution time series. When regularly sampled data is required, as for some spectral analysis, data gaps were filled with a constant value to minimize spurious peaks in spectral analysis. The value assigned to a gap was calculated by taking the mean of the salinity 4 days on each side of the gap.

### 3.2. Satellite Imagery

[22] A series of 92 images were obtained from the Moderate Resolution Imaging Spectroradiometer (MODIS) instrument aboard the Aqua spacecraft. Though an image is available from MODIS at a given location every 1 or 2 days, only 92 images were free of clouds and coincided with days in which ferry data was available. We used the narrow band (~10 nm) 1 km images at 551 nm. They were spatially subsetted to include the Straits of Georgia and Juan de Fuca. Default calibration factors were used to process the files into Level 2 products giving top of atmosphere leaving radiance. The images chosen nearly span the ferry program, from 4 February 2003 until 24 April 2006. Every image was taken between 1245 and 1430 local time.

[23] River plumes are generally more reflective than sea water at visual wavelengths [*Kirk*, 1994; *Li et al.*, 2003] because they contain a higher concentration of suspended sediments. We found the highest contrast between SoG water and Fraser River plume water at 551 nm. The plume was chosen in each image semiautomatically. More objective methods may be desirable [e.g., *Thomas and Weatherbee*, 2006], but the variability in the plume spectral signature and the manageable number of files made it unnecessary. We justify our method because comparisons of ferry salinity and satellite radiance showed a good correlation, with high radiance corresponding to low salinity. The correlation indicates that the ferry and satellite measure the same plume (i.e., the sediment and salinity plumes represent the same water mass).

## 4. Results

### 4.1. Horizontal Plume Salinity Structure

[24] Visual examination of some of the 8502 ferry transects reveals a large degree of variability, both in the along-strait salinity structure, and in a time series of salinity at any point in the transect. The mean plume structure is shown in Figure 3, formed by averaging all of the ferry transects. The lowest mean salinity is 22 PSU, found at along-track distance 16 km, which is the closest point of the transect to the mouth of the Fraser River (see Figure 1). The distance between this point and the westbound transect is typically 5.5 km and the distance from this point to the eastbound transect is 8.9 km. This feature will be referred to as the plume "core." The average along-strait extent of the plume, bounded by the region of near-constant salinity at the

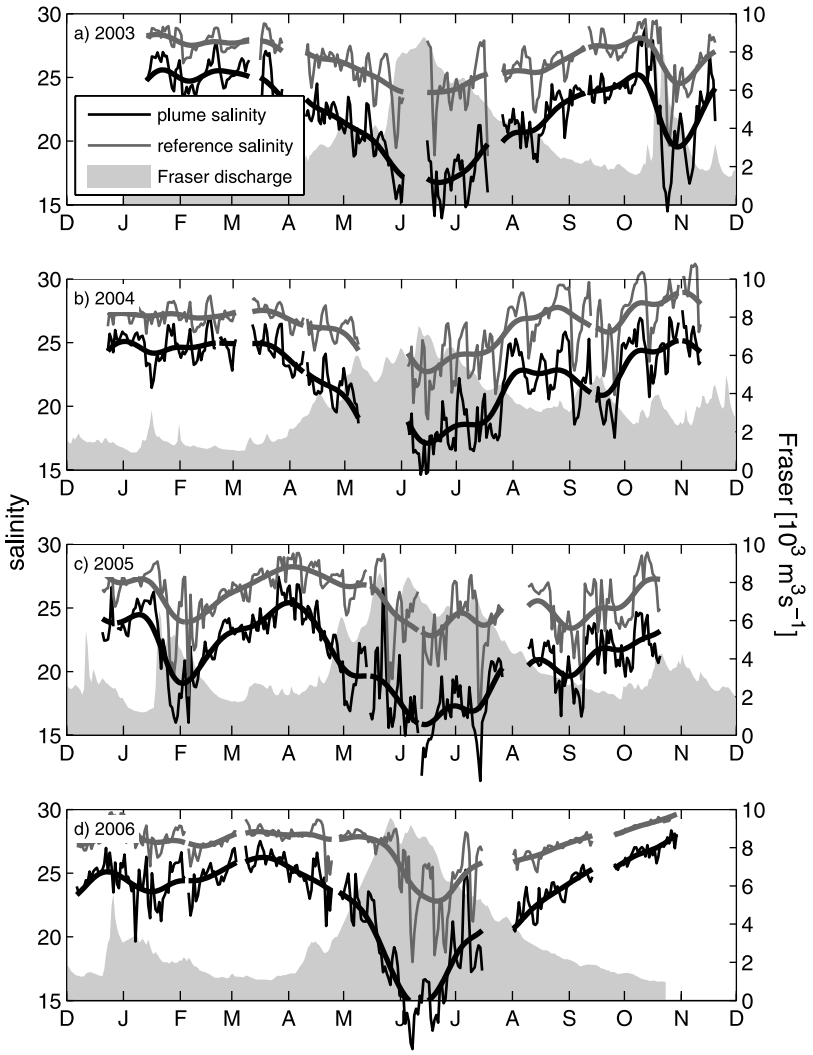


**Figure 4.** Full time series of mean daily plume salinity (black line) and reference salinity (gray line). The heavy lines are salinity filtered with a 25 day Hamming window. The shaded curve is the Fraser flow at the mouth. Each panel is a year of data: (a) 2003, (b) 2004, (c) 2005, and (d) 2006.

western edge, is 45 km from the reference distance and 33 km from the river mouth. Outside of the plume the mean salinity is 26.5 PSU. This water will be referred to as the reference salinity or SoG surface water. The salinity gradient on both sides of the plume core is 2.2 PSU/10 km. We note that the horizontal salinity gradient of the mean transect is much weaker than the gradient in any single transect. The plume front changes location on the basis of the external forcing and averaging over many tracks lessens the gradient (note the sharp gradients in the single transect shown in Figure B1).

[25] Deviations from the mean salinity transect may be substantial. The distribution of salinity at any location is not symmetric about the mean transect. Fresh anomalies have a greater excursion from the mean than saline anomalies, thus we present the 5, 25, 50, 75 and 95% percentiles in Figure 3 to quantify the variability. The distribution of salinity is widest at the core of the plume and narrows toward either end. At the core of the plume, only 5% of the observations had a salinity less than 12 PSU and the minimum salinity at this point is near 5 PSU. Only 5% of the measurements at the core of the plume exceed 28 PSU, larger than the mean reference salinity. By definition this is not plume water, but such a salinity is possible if the plume happens to be outside the ferry track. The reference salinity is rarely lower than 22 PSU or greater than 29.5 PSU.

### 4.2. Plume Salinity

[26] The nature of the ferry track does not allow us to compute a true spatial mean of the plume salinity (e.g., the volume average of salinity within some isohaline). Instead we define a mean salinity equal to the spatial average of the section of the ferry transect within the plume. We expect our definition to be a meaningful proxy for the true mean plume salinity based on comparisons with 48 CTD profiles taken in the plume over the years 2002–2005. The profiles were taken semiregularly at a hydrographic station 4.5 km from Sand Heads (Figure 1). They show that the plume depth, defined as the base of the strongly stratified surface layer, ranges from 4 to 8 m. As the ferry samples at about 2 m (i.e., a depth less than or half of the plume thickness), and the salinity profiles are linearly stratified, the ferry effec-

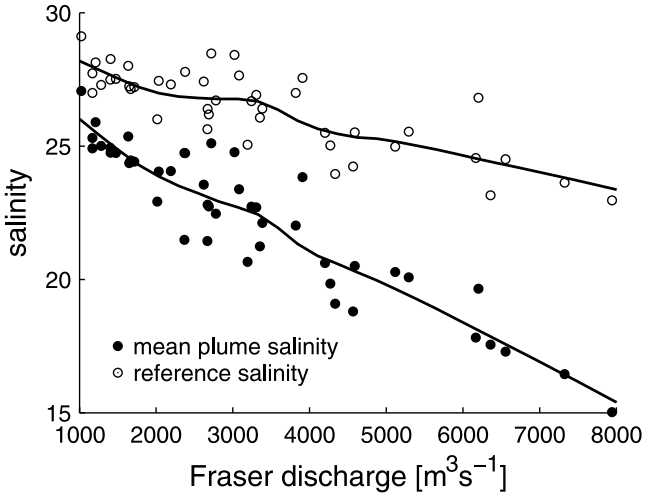


**Figure 5.** Fraser plume salinity (solid circles) and reference salinity (open circles) as functions of Fraser River discharge. The regression is between the 25 day filtered time series of salinity and the 25 day filtered time series of river discharge. The solid lines illustrate the regressions and were estimated by the LOESS algorithm.

tively measures the vertical mean. The potential error introduced by this assumption is relatively small. For example, if the salinity linearly increases from 20 to 30 over 10 m, the 2 m salinity is 10% smaller than the mean salinity.

#### 4.2.1. Subtidal Variations

[27] Figure 4 shows the complete daily binned time series of plume and reference salinity. Each panel shows 1 year of data. We anticipate the Fraser River to be important in setting the salinity and thus include a time series of discharge at the mouth as the shaded area. Three trends immediately stand out: the strong covariance of the plume and reference salinity with river discharge, the 10–20 day fluctuations superimposed on the seasonal changes, and the correlation of reference salinity with plume salinity. We include 25 day low-pass filtered curves of salinity in Figure 4 (thick lines) to illustrate the seasonal changes. The freshest water occurs early in June during the freshet. At this time the reference salinity can be as low as 20 PSU and the plume salinity as low as 10 PSU. Other significant discharge events, such as in October 2003 and January 2005, can drive the reference and plume salinity to freshet levels. During low-flow periods (e.g., late fall) the reference salinity is roughly 28 PSU and the plume salinity is near 25 PSU.

[28] The time series of plume salinity suggests that the Fraser river correlates with plume and reference salinity, but only on time scales greater than about 15 days. Figure 5 shows the reference salinity and plume salinity as a function of Fraser river discharge at the mouth. Each time series has been filtered with a 25 day Hamming window and subsampled to remove autocorrelation. The solid lines are calculated with LOESS, a nonparametric data smoother [*Cleveland*, 1979]. The salinity of each decreases quasi-linearly with increasing discharge, the plume salinity decreasing more sharply.

[29] The time series of plume salinity (Figure 4) appears to contain a periodic component on 10–20 day scales superimposed on the Fraser discharge signal. To examine this in more detail, Figure 6 shows a variance-conserving power spectrum of the daily mean plume salinity. The spectrum was computed with the Welch method [e.g., *Percival and Walden*, 1993] using a 200 day Hamming window with a 50% overlap yielding 26 effective degrees of freedom. The $2\sigma$ intervals around the spectrum were derived from the distribution of Monte Carlo realizations. Also shown is the power spectrum of the Fraser River discharge

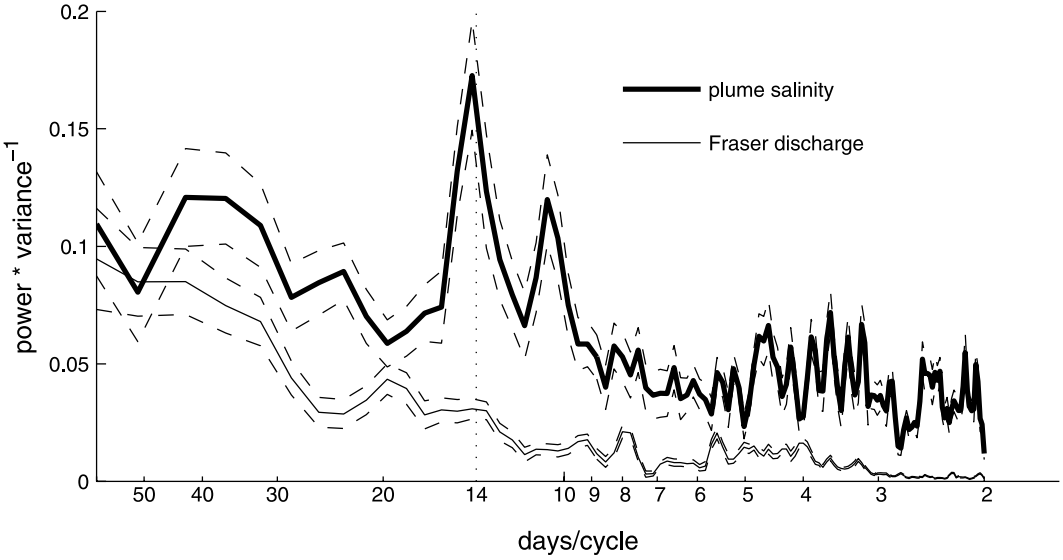


**Figure 6.** Variance conserving spectrum of the mean plume salinity (thick solid line) and the Fraser River discharge (thin solid line) with their respective $2\sigma$ confidence intervals. Both spectra were calculated using the Welch method with a 200 day window and 50% overlap, yielding 26 effective degrees of freedom.

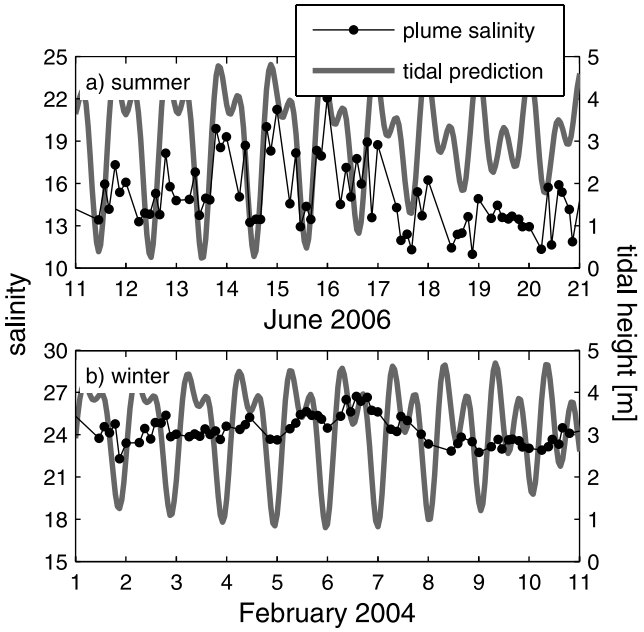


**Figure 7.** Time series of plume salinity (open circles and solid dark line) and predicted tidal height at Point Atkinson (solid gray line). Each panel displays 10 days of ferry data: (a) 10 days in mid-June 2006, during high river discharge ($\sim$8500 $m^3$ $s^{-1}$), and (b) 10 days in February 2004, during low river discharge ($\sim$1300 $m^3$ $s^{-1}$). Note the smaller variance in plume salinity during winter and the lower sensitivity to the large diurnal ebb tides.

calculated with the same window parameters. Notable peaks in plume salinity appear at $\sim$35, 14 and 10.7 days. The broad peak at 35 days is caused by the 30–40 day long gaps in the time series which appear when the ferry is taken off route for its annual refit. The physical cause of the peak at 10.7 days is unclear. If spectra are computed with 1 year of data, instead of the full 4 years, the peak at 10.7 days only occurs in 2005 (whereas the peak at or near 14 days occurs each year). The peak in salinity spectral energy at 14 days and the lack of a similar cycle in the Fraser spectrum suggest that the plume salinity may be influenced by fortnightly cycling in tides, and will be investigated further in section 5.1.2.

#### 4.2.2. Tidal Variations

[30] To determine the importance of tides on daily time scales we make use of the high-resolution ferry time series. A time series illustrating the importance of individual ebb and flood cycles on plume salinity is shown in Figure 7. Figure 7a plots the ferry salinity and the tidal height at Point Atkinson over a period of 10 days in June 2006, while Figure 7b shows a period of 10 days in February 2004. In the summer, the most striking trend is the decrease in salinity found at lower-low water. Higher-low water also corresponds to local minima in salinity. The change of salinity from higher-low water to lower-low water can reach 5 PSU. The tidal nature of the plume salinity appears to be seasonally modulated, as Figure 7b shows less variation over a tidal cycle. The salinity at lower-low water may be up to 2 PSU lower than during other times in the tidal cycle.

[31] We make use of the Lomb-Scargle method [*Lomb*, 1976; *Scargle*, 1982] to study the frequency composition of the high-resolution plume salinity time series. A standard spectral estimator could not be used because the ferry sailings are not spaced at regular intervals. The oversampling factor was set to 4 (corresponding to about 1/2 h), and we use the full time series to gain the highest possible frequency resolution, $\Delta f$ = 1.8038 x $10^{-4}$ cycles/d. The resulting periodogram is shown in Figure 8, but the frequency axis is limited to focus on the semidiurnal (Figure 8a) and diurnal (Figure 8b) tidal frequencies. The 99% significance level for spectral lines is shown by the horizontal broken line. Statistically significant peaks tend to cluster around frequencies of one, two, four, and five times daily, fortnightly, semiannually, and annually. Annual and semiannual peaks are caused by the river freshet, while the fortnightly peaks are expected on the basis of the 14 day cycle observed in the Welch periodogram (Figure 6) of daily binned salinity. The cycles at four and five per day are caused by fact that the eastbound and westbound ferry tracks are not exactly colocated (Figure 1) such that the ferry's westbound track lies closer to the Fraser River mouth than the eastbound track. The proximity causes the westbound tracks to have a lower salinity (average of 1 PSU over the whole time series). Because the westbound sailing departs every 5 h, a cycle is created at 4–5 $d^{-1}$.

[32] Every statistically significant diurnal and semidiurnal peak in the plume salinity occurs at a known tidal frequency except for the peak at 24.092 h. Here we define the known tidal frequencies to be the 67 constituents which would be used in a harmonic analysis of a 1 year time series with the MATLAB fitting software, T_TIDE [*Pawlowicz et al.*, 2002]. However, there is not a significant cycle in salinity at the frequency of every tidal constituent. The line heights relative to $M_2$ of all statistically significant peaks are listed in Table 1 along with the elevation amplitude of the respective tidal constituent. We also include constituents with elevation amplitudes exceeding 5% of $M_2$, though their line heights in salinity were not significant. In anticipation of the discussion on the importance of ebb/flood cycles on plume salinity, the amplitude of each constituent multiplied by its period is included in Table 1. This quantity will be used as a proxy for the horizontal excursion by the constituent, and will be discussed in detail in section 5.1.2. Within the diurnal band, significant spectral power was found at the frequencies of $K_1$, $P_1$, $O_1$, $\psi_1$, and $\pi_1$. The peak at $Q_1$ was not significant. In the semidiurnal band, the power at $M_2$, $K_2$, and $T_2$ is significant, while the power at $S_2$ and $N_2$ is not.

[33] In the salinity spectrum, $K_1$ is three times higher than $M_2$, and is the strongest line in the semidiurnal and diurnal bands. In terms of elevation, $K_1$ is 95% of $M_2$. In salinity, the line heights at $P_1$ and $O_1$ are 139% and 78% of $M_2$, which are proportionately higher than their constituent amplitudes in elevation. Only $Q_1$ is smaller in salinity than elevation. Somewhat unexpectedly, energy appears in salinity at the frequencies of $\psi_1$ and $\pi_1$, which are negligible in terms of the elevation spectrum. In the semidiurnal band, the plume salinity line height at $S_2$ and $N_2$ are 8% and 3%, respectively, of $M_2$, and are below the 99% significance level, despite their importance in tidal elevation. The energy at $K_2$ is 78% of $M_2$, though it is only 7% of $M_2$ in elevation.

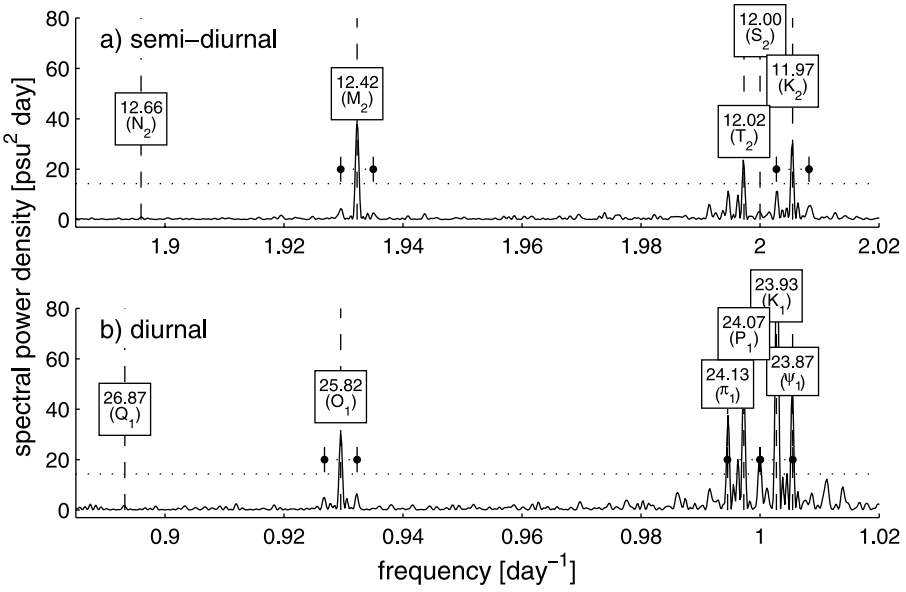


**Figure 8.** Lomb-Scargle periodogram of plume salinity focused on (a) the semidiurnal band and (b) the diurnal band. The period of each constituent, in hours, is given above its name. Small dots with the vertical solid lines show the sidebands produced by a yearly modulation about the peak on which they are centered. The dashed line shows the 99% significance level. Energy at K1 extends well beyond the *y* axis upper limit.

Finally, the energy at $T_2$ is 62% of $M_2$, even though it is a very small constituent in elevation with ~2% of $M_2$.

### 4.3. Plume Surface Area

[34] It is possible to estimate the surface area of the plume with a combination of ferry data and satellite images. The ferry track cuts a straight line through the plume. A simple estimate of area can be made by assuming the ferry measures the diameter of a semicircular plume [*Pawlowicz et al.*, 2007]. However, visual inspection of the MODIS images and previous studies [e.g., *Tabata*, 1972] show that the plume can take on a myriad of shapes. Even so, the length of the ferry track inside the plume should be roughly proportional to the plume surface area. Instead of assuming a particular geometry, the ferry time series of squared length was compared to a time series of area obtained from a series of 92 MODIS images. A regression between the time series of low-pass filtered ferry squared length and satellite measured area was obtained by determining the principal eigenvector of a singular value decomposition analysis. It is this regression that determines the plume geometry and thus the scale factor to apply to the ferry data. For our study, the results of the regression are:

$$A_{plume} = -725 + 1.42L_{ferry}^2 \quad (1)$$

where $L_{ferry}$ is the length of the track within the plume measured by the ferry.

[35] The final ferry time series, scaled by (1), appears in Figure 9, along with the satellite area and Fraser River discharge. The most outstanding feature is the variability in the plume area. For example, in September 2003, the estimated area varies from <0 to 1000 km$^2$ (note that the plume can have a negative area; this is just a by-product of the regression with satellite area which was allowed an offset). We note that some of the variability in plume area is likely caused by the ability of our algorithm to properly find the plume within the transect given the variability in the along-track structure (Figure 3) and a geometrical scaling factor which likely varies in time. Also, we note that the plume may be advected by wind and tides relative to the ferry track, altering our estimate of plume surface area. A low-pass filtered time series (25 day Hamming window) is presented along with the original time series to remove the variability. Plume area varies from 400 km$^2$ or less during low-flow periods to as much as 1,700 km$^2$ during strong freshets. Variability in the time series, quantified with ±2 standard error curves centered on the low-pass time series in Figure 9, is such that the effects of small fluctuations in river discharge are unclear. Only freshets and other large

**Table 1.** Comparison of Line Heights at Various Tidal Frequencies in the Salinity Spectrum With the Constituent Elevation at Point Atkinson, BC[a]

| Constituent | Elevation at Point Atkinson | Constituent Horizontal Excursion[b] | Salinity Line Height |
|---|---|---|---|
| $M_2$ | 1.00 | 1.00 | 1.00 |
| $S_2$ | 0.25 | 0.24 | 0.08[c] |
| $N_2$ | 0.20 | 0.20 | 0.03[c] |
| $K_2$ | 0.07 | 0.07 | 0.78 |
| $T_2$ | 0.02 | 0.01 | 0.62 |
| $K_1$ | 0.94 | 1.81 | 2.89 |
| $O_1$ | 0.53 | 1.10 | 0.78 |
| $P_1$ | 0.29 | 0.56 | 1.39 |
| $Q_1$ | 0.08 | 0.17 | 0.04[c] |
| $\psi_1$ | 0.02 | 0.04 | 0.99 |
| $\pi_1$ | 0.02 | 0.03 | 1.31 |

[a]All quantities are given as ratios to $M_2$.
[b]Constituent horizontal excursion is an estimate of the horizontal displacement caused by the constituent over its tidal period.
[c]Not significant at 99% significance level.

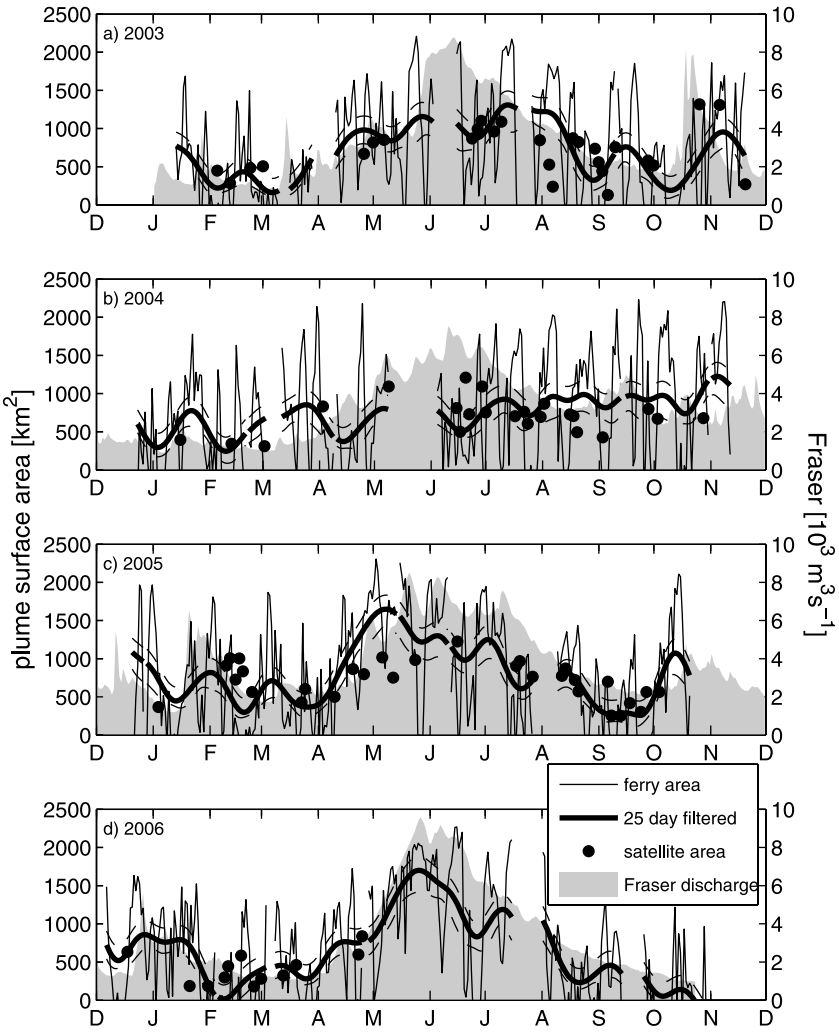


**Figure 9.** Each panel is a time series of daily mean Fraser River plume surface area: (a) 2003, (b) 2004, (c) 2005, and (d) 2006. The surface area has been scaled by a linear regression to the satellite area time series (solid circles). The thin line is the daily mean area, while the heavy line is the area filtered with a 25 day Hamming window. The thin broken curves surrounding the filtered time series are the ±2 standard error bounds. The Fraser River discharge at the mouth is shown in solid gray.

discharge events (e.g., October 2003 and January 2005) cause statistically significant changes in surface area.

[36] The time series of low-pass filtered plume surface area reveals that the Fraser River appears to set the seasonality in the plume area. To investigate the effect of the Fraser River directly, we plot the plume area as a function of the river discharge (Figure 10). Instead of plotting the original time series, 25 day Hamming window filtered and decimated versions of each are shown. The surface area increases with increasing river discharge, but unlike salinity, which varies quasi-linearly with discharge (Figure 5), the nonparametric fit suggests the area varies proportionately less at high discharge than at low discharge.

## 5. Discussion

### 5.1. Controls of Plume Salinity

#### 5.1.1. River Discharge

[37] On time scales greater than about 15 days, both the plume salinity and reference salinity decrease linearly with increasing river discharge. Plume salinity decreases at 1.4 PSU per 1000 $m^3s^{-1}$, while the reference salinity decreases at a half the rate, 0.7 PSU per 1000 $m^3s^{-1}$. Because their respective slopes differ, the salinity gradient between them increases with discharge. The plume salinity is 2 PSU fresher than the reference salinity at minimum river discharges, and 8 PSU fresher at maximum flow.

[38] The direct comparison of a spatial mean of plume salinity to river flow presented in Figure 4 is the first to the authors' knowledge. The mean salinity has a special significance because, with some assumptions, it is essentially a measure of the fresh water content in the plume. If the depth of the plume does not vary with river flow, and if the ferry transect is representative of any transect through the plume, our linear track mean becomes a volume mean. With these first-order assumptions, we conclude the Fraser plume contains a higher proportion of fresh water relative to reference water during high river flow than during low river flow. Furthermore the fresh water residence time, defined as the total volume of fresh water divided by input

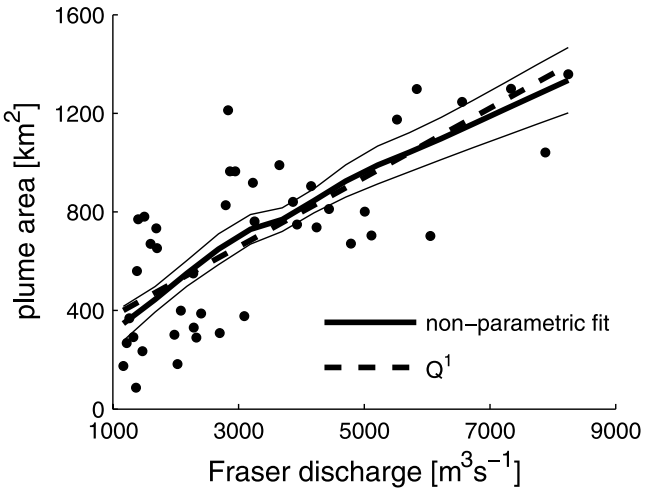


**Figure 10.** Relationship between 25 day filtered plume surface area and 25 day filtered Fraser River discharge (solid circles). A LOESS nonparametric fit (thick solid line) along with the $1\sigma$ bootsrapped fit error (thin solid lines) is used to test if the data are consistent with a straight line fit (thick dashed line).

of river flow, is roughly independent of river discharge, because the surface area increases with increasing river discharge. *Pawlowicz et al.* [2007] quantify this with ferry data in the Fraser plume and calculate a fresh water residence time of about 1 day.

[39] *Royer and Emery* [1982] observe a correlation between Fraser river discharge and surface salinity on ferry routes north and south of our ferry route. They measure a lag of up to 3 days between river discharge and salinity. We do not observe a lag in our daily binned data, presumably because we sample closer to the river mouth. Comparison of Figure 3, the salinity time series given by *Royer and Emery* [1982] with Figure 4, suggests that their plume is our reference salinity because the range in salinity is similar.

[40] Other systems show a freshening with increasing river discharge. For example, Figure 6 of *Geyer et al.* [2000] shows an inverse relation between the salinity 12 km from the river mouth in the Eel River plume and the river discharge. The surface salinity in Amazon River plume shows a seasonal signal, as the low-salinity contours are pushed seaward during winter-spring high flows compared to summer-fall low flows [*Lentz*, 1995b].

[41] Finally, we address the correlation between river discharge and reference salinity. The reference salinity is not simply the nominal SoG water into which the plume propagates. The correlation between Fraser discharge and reference salinity (Figure 5) is explained by two factors. First, rivers which discharge into the SoG have a discharge cycle which resembles the Fraser, a fact exploited by *Pawlowicz et al.* [2007] to scale the Fraser discharge to the total fresh water input into the SoG. Second, the plume must lose water through the plume front to conserve volume because it gains water from the river and entrains through the base. Water that has been fluxed through the plume front joins the SoG surface water, or reference water. Because the Fraser river flow constitutes at least half of the total fresh water input into the SoG, the water fluxed through the front will partly determine the reference salinity.

### 5.1.2. Tides

#### 5.1.2.1. Fortnightly Cycle

[42] The 14 day cycle in plume salinity (Figure 6) is particularly interesting because it is an important subtidal time scale for estuaries. To quantify the relationship between the fortnightly tidal cycle and the plume salinity, a daily measure of the strength of the tide was needed. We chose to use the maximum daily tidal range, or the difference in height between higher-high water and lower-low water. The squared coherence and phase between tidal range and filtered plume salinity was computed by using spectra and cross spectra obtained with Welch's method with a 100 day Hamming window. When the full ferry time series was considered, the maximum squared coherence was 0.34 at 14 days, significant above the 95% level. The 14 day peak was broad, reaching zero coherence at 10 and 20 days. The phase shift was not discernible from zero so that local maxima in salinity were in phase with maxima in daily tidal height.

[43] Visual inspection of a time series of maximum daily range and plume salinity suggest that the their relationship is stronger in the summer than in other seasons. To quantify the seasonal change in the coherence between fortnightly tidal cycling and plume salinity, the full time series was split into 50% overlapping, 184 day segments. The coherence band-averaging used 46 day Hamming windows overlapped by 50%. Figure 11 plots the coherence in each segment as a time series along with the Fraser discharge. The squared coherence is 0.4 or higher and statistically significant in and around the freshet, but is low and statistically insignificant during low river flows.

[44] The change in Fraser plume salinity as a function of the fortnightly tidal cycle may be expected on the basis of the results of *Geyer and Farmer* [1989]. In the Fraser

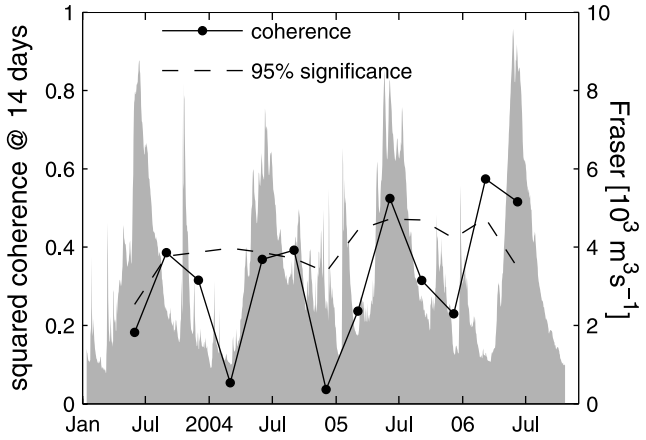


**Figure 11.** Time series of squared coherence at 14 days between maximum tidal height and plume salinity (solid line and open circles). The dashed lines show the 95% significance level from the coherence analysis. Each point is plotted at the center of a 184 day segment over which the coherence was computed. Adjacent segments were overlapped by 50%, introducing some autocorrelation. The shaded area shows the Fraser River discharge at the mouth.

estuary, the intensity of mixing at the salt wedge is a function of the tides. During the flood tide, the salt wedge advances upriver and is stably stratified. During an ebb tide, shear increases on the salt wedge halocline until instability mixes fresh water downward and salt water upward. *Geyer and Farmer* [1989] hypothesize that the amount of mixing should be proportional to the strength of the ebb, and therefore to fortnightly cycling. Strong ebbs, characteristic of spring tides, would more effectively break down the salt wedge, increasing the upward flux of salt. In other estuaries, the fortnightly cycle in mixing has been observed directly. In the Hudson River estuary, *Peters* [1997] finds an insignificant vertical turbulent salt flux across the halocline during neap period ebbs, but a significant flux during spring period ebbs. In the Columbia River Estuary, *Jay and Smith* [1990] find the stability of the salt wedge to be sensitive to spring/neap cycling, but add that the sensitivity is a function of the river flow. At the highest river flows, the stratification is strong enough to withstand shearing, and the salt wedge is broken down during most ebb tides during low-flow periods. *MacCready et al.* [2002] present a highly simplified conceptual model of the fortnightly cycle of estuarine structure, useful in the present case to elucidate the mechanism behind the fortnightly cycle in plume salinity. During the well-mixed state (spring tides), relatively high salinity water exits the estuary at the surface, while during the stratified state (neap tides), relatively fresh water exits at the surface. The Fraser Estuary, however, restratifies much faster than the *MacCready et al.* [2002] model, and during spring tides it does not remain fully mixed during all phases of the tide.

[45] On the basis of the studies in the Fraser, Columbia, and Hudson River estuaries, we suggest that the 14 day cycle in plume salinity observed in the Fraser plume is caused by the fortnightly cycle of mixing in the estuary. Ebb tides during times of maximum tidal amplitude in the fortnightly cycle would create a higher upward salt flux than weak ebb tides. The increased upward flux exports higher-salinity water out of the estuary in the seaward moving upper layer. When ebb tides are weak, the shear is not strong enough to break down stratification. Thus upper layer water glides over the salt wedge, exits the estuary with relatively little mixing, and becomes the plume.

#### 5.1.2.2. Ebb/Flood Cycles

[46] The Lomb-Scargle periodogram (Figure 8) illustrates the tidal nature of the plume. The periodogram revealed two key features: First, the relative strength of the diurnal lines compared to the semidiurnal lines, and second, the existence of lines in the salinity spectrum at frequencies of minor tidal constituents.

[47] Here we develop a simple conceptual model to explain the relative strength of the diurnal lines to the semidiurnal lines. The salinity in the upper 5 m of the water column at a mooring 6.3 km directly seaward from the Fraser River mouth was shown by *Crean et al.* [1988] to be highly influenced by tides (we note in addition that the river discharge was high during their study). *Geyer and Farmer* [1989] and *Kostaschuk and Atwood* [1990] have shown that the salt field is advected up to 20 km during a tidal cycle. Therefore we take advection of a horizontal salt field as the dominant process setting the plume salinity field on tidal time scales. If each tidal constituent independently contributes to the total advection, we can estimate a per constituent excursion by integrating its velocity over the ebb phase. However, tidal currents are not available near the Fraser River mouth, so we use tidal amplitude as a proxy for velocity. This approximation is roughly justified in the southern SoG on the basis of the model results of *Foreman et al.* [1995]. At Tsawwassen (gauge 20), the ratio $K_1/M_2$ is 1.03 in terms of elevation. Offshore of Tsawwassen in midstrait (station d), the ratio $K_1/M_2$ is 0.68 in terms of velocity. Therefore, because velocity is proportional to amplitude, excursion becomes the period of the constituent multiplied by its elevation. The results for each constituent are given in Table 1. The longer period of the diurnal constituents amplifies their importance, which is the general behavior seen in the plume salinity spectrum where the diurnal lines are typically higher than the semidiurnal lines. For example, the ratio $K_1/M_2$ is 2.89 in salinity and 1.81 in excursion, but only 0.94 in elevation. As with $K_1$, the strong lines at $P_1$ and $O_1$ relative to $M_2$ reflect their importance in terms of excursion in our simple model.

[48] The amplification of diurnal lines was also found further away from the Fraser river mouth in the ferry time series of *Royer and Emery* [1982]. As the tide ebbs the southward streaming currents advect the plume southward into the southern ferry track (see *Royer and Emery* [1982, Figure 1] for a map of the route). The decrease in salinity by advection is enhanced by the increase of river discharge caused by the ebbing tide. Qualitatively our results are consistent. However, our ferry route is measuring changes of salinity within the plume itself whereas *Royer and Emery* [1982] observe changes as the plume is advected into the ferry track.

[49] The existence of lines in the plume salinity spectrum at the frequencies of tidal constituents with very small or negligible amplitudes ($\psi_1$, $\pi_1$, and $T_2$) is caused by the Fraser River's strong annual effect on plume salinity. These lines can be understood in terms of the effects of modulating a high-frequency signal (the "carrier," here the diurnal and semidiurnal cycles), by a low-frequency signal (here the Fraser annual cycle). When the modulation is by an annual cycle, the sidebands will lie $\Delta f = 1/365\ \mathrm{d}^{-1}$ on each side of the carrier, potentially interfering with peaks of true astronomical origin. Astronomically, $T_2$ is the major elliptic wave of $S_2$, $\psi_1$ is the elliptic wave of $K_1$, and $\pi_1$ is the elliptic wave of $P_1$ [e.g., *Melchior*, 1966].

[50] To investigate the effect of an annual modulation on diurnal and semidiurnal cycles in plume salinity, Figure 8 contains marks identifying the locations where annual sidebands should occur for the lines at the $M_2$, $K_2$, $O_1$, $P_1$, and $K_1$ frequencies. The markers are centered about the main peaks and denoted by small dots with vertical lines. Each tidal frequency marked with 1 year modulations shows sidebands, but not all sidebands are statistically significant. In the diurnal band, the significant energy at $\psi_1$, and $\pi_1$ (and the nontidal 24.00 h line) are sidebands of $K_1$ and $P_1$. In the semidiurnal band, the $T_2$ line height is significant. Energy appearing at $T_2$ could be an annual sideband of $S_2$, but the energy at $S_2$ is only 8% of $M_2$. Thus it is not clear why the line height of $T_2$ is as high as it is.

#### 5.1.2.3. Seasonality of Tidal Effects

[51] Figures 7 and 11 reveal that the effect of tides on the Fraser plume salinity is a function of river discharge. Tidal

variations in salinity are maximized during high river flow and minimized during low flow. To explain this observation, the effects of river discharge on the estuarine salt field must be considered.

[52] Estuarine salinity structure varies with river discharge and tides. In steady state (zero net salt flux), river flow sets the length of the salt intrusion and vertical stratification [*Hansen and Rattray*, 1965; *Chatwin*, 1976]. Time-dependent behavior becomes important when the forcing time scale is equal to or less than the adjustment time scale [*Hetland and Geyer*, 2004]. *Kranenburg* [1986] shows that the adjustment time is a function of river discharge and length of an estuary, and that it is a fraction of the "fresh water advective time scale," $\tau_f = L/u_f$, where $L$ is the length of the salt intrusion and $u_f$ is the fresh water velocity.

[53] Utilizing the results for the structure of an estuary based on the work of *Hansen and Rattray* [1965], *Chatwin* [1976], and *Kranenburg* [1986] along with the work specific to the Fraser estuary by *Stronach* [1981], *Crean et al.* [1988], *Geyer and Farmer* [1989], and *Kostaschuk and Atwood* [1990], we describe a conceptual model for the combined effects of tides and river flow on the plume salinity. The model will be discussed in terms of the differences between winter and summer flows.

[54] In winter, *Kostaschuk and Atwood* [1990, equation (1)] predict that the tip of salt wedge will be located 36 km upriver at high water and 21 km upriver at low water, meaning the salt wedge is always upstream of the river mouth. This suggests that water at the river mouth will always be mixed because most mixing occurs at the salt wedge. Water mixed into the upper layer will have a relatively high salinity because the salt wedge salinity is higher in winter than summer [*Stronach*, 1981]. The effects of tides on salinity should be minimal, because a single tidal cycle will only advect mixed water up and down the river near the mouth while the stronger salinity gradients remain upstream. Fortnightly changes in the strength of mixing on the ebb tide may be important, but water at the river mouth and in the plume will always be mixed because it is further downstream of the salt wedge in winter than in summer.

[55] In summer, the plume has a lower salinity because more fresh water is coming from the river, and because the salt wedge has a lower salinity than in winter [*Stronach*, 1981]. The tidally averaged length of the salt intrusion will be shorter in summer because the river discharge is higher, creating a smaller surface area for mixing. Tidal effects will be stronger, because the salt wedge will lie 18 km upriver from the river mouth at high water and at the river mouth at low water. At low water the salt wedge is essentially flushed out of the river, which brings relatively fresh water to the near-field plume. The effect will be particularly strong once per day because the excursion due to $K_1$ is twice as large as $M_2$. During strong ebbs in the fortnightly cycle, mixing is enhanced, and the plume salinity will be, on the average, a few PSU higher than during weak ebbs.

### 5.2. Controls on Plume Area

#### 5.2.1. River Discharge

[56] Considerable variability characterizes the daily plume surface area time series (Figure 9), most of which lies in a frequency band not associated with physical forcing. Therefore much of it is likely caused by the shortcomings of using a 1-D ferry transect or by limitations of the plume finding algorithm. Previous estimates of surface area in other systems have also contained significant errors. *Garvine* [1975] estimates the Connecticut River plume surface area with a series a 1-D transects, and while it is clearly correlated with river flow, significant unexplained variability remains. However, after removing variations of less than 25 days, the surface area of the Fraser River plume clearly increases with river flow. A linear regression shows that the area increases from 400 km$^2$ to 1400 km$^2$ at rate of 140 km$^2$ per 1000 m$^3$ s$^{-1}$. While a straight line fit appears to describe the relationship well, the nonparametric fit in Figure 10, is slightly concave downward.

[57] The suitable theory for determining the relationship between surface area and river discharge will depend in part on the dynamics of the plume at the mouth. The mouth Rossby number, $R_o = U/fL_{mouth}$, calculated using the mean annual fresh water outflow and mouth dimensions in *Geyer and Farmer* [1989], is 4.4. The mouth Kelvin number, $K_m = L_m/L_d$, where $L_d$ is the deformation radius ($\sim$7 km), and $L_m$ is the width of the river mouth [*Garvine*, 1987], is roughly 0.13. Both numbers indicate rotation will be unimportant at the river mouth.

[58] The effects of buoyancy relative to momentum will become evident at a distance $l_m = M^{3/4}B^{-1/2}$ from the river mouth, where $M$ and $B$ are the initial fluxes of momentum and buoyancy, respectively [*Fischer et al.*, 1979]. To estimate this distance, the momentum flux is written as $UQ$, and the buoyancy flux written as $g'Q$, where $U$ is the river inflow velocity, $Q$ is the volume flux of fresh water, and $g'$ is reduced gravity. After substitution, the length scale becomes:

$$l_m = \frac{U^{3/4}}{g'^{1/2}} Q^{1/4}. \tag{2}$$

In estimating $l_m$ we use the observed minimum and maximum river discharge, measurements of the outflow velocity at or near the river mouth from *Ages* [1979] and *MacDonald and Geyer* [2004], and assume $g'$ ranges from 0.1 to 0.2 m s$^{-2}$. In the Fraser plume, $l_m$ ranges from 20 m (winter) to 36 m (summer). This very short distance suggests that buoyancy forcing is always important, and that water issuing from the mouth will not behave as a pure jet.

[60] Further away from the mouth, rotational effects are evident in aerial photographs [*Tabata*, 1972] and drifter tracks [*Crean et al.*, 1988]. Idealizing a river plume as an anticyclonic rotating bulge in cyclostrophic balance, without rotation, *Yankovsky and Chapman* [1997] find a bulge radius

$$r_s = R_d \frac{(3 + F^2)}{(2 + F^2)^{1/2}}, \tag{3}$$

where $R_d$ is the outflow internal deformation radius, $(g'h_o)^{1/2}/f$, $F$ is the outflow Froude number, $U/(g'h_o)^{1/2}$, $h_o$ is the outflow depth, and $g'$ is the reduced gravity. When the inflow is weak or the density difference large ($F \ll 1$), the bulge radius is $4.24R_d$, while for strong flows or small density differences ($F \gg 1$), the bulge radius is $Uf^{-1}$.

[61] From the plume area time series (Figure 9), the length scale of the plume, assuming it is a semicircle for simplicity, ranges from 16 km (winter) to 32 km (summer). If $F \gg 1$ for the Fraser outflow, then $r_s$ would range from 10 km ($U = 1$ m s$^{-1}$, $f = 10^{-4}$) to 20 km ($U = 2$ m s$^{-1}$), smaller than the observations. If $F \ll 1$, $r_s$ ranges from 19 km (winter: $\Delta S = 5$, $h_o = 5$ m) to 32 km (summer: $\Delta S = 15$, $h_o = 5$ m), in closer agreement to our observations.

[62] The low-Froude-number limit is likely more appropriate even though the observed outflow is supercritical at the mouth [*MacDonald*, 2003] because dissipative processes and mixing in the near-field plume [*Cordes et al.*, 1980; *MacDonald et al.*, 2007], not accounted for in the theory, quickly reduce the flow speeds. Taking the reduced gravity to be proportional to river discharge (as was shown in Figure 5), we find that the plume area then varies linearly with discharge and outflow depth, $A \propto Qh_o$. The straight line fit in Figure 10 falls within the $1\sigma$ error of the nonparametric fit, suggesting the *Yankovsky and Chapman* [1997] model is appropriate, though we note the curvature in the nonparametric fit more closely follows a $Q^{1/2}$ dependence. Such a scaling was also found by *Warrick and Fong* [2004] for other plumes, but this was derived by squaring the buoyant jet length scale (2), which is not appropriate in this case because $l_m$ is so small. It is possible that variations in the outflow depth $h_o$ can account for this difference but we cannot easily test this. However it should be noted that the Fraser plume, with its short residence time [*Pawlowicz et al.*, 2007], is not really in steady state [see also *Hodgins et al.*, 1994], so the rotating bulge idealization may not be as useful as it is in other situations [e.g., *Chant et al.*, 2008].

#### 5.2.2. Tides

[63] The time series of plume area (Figure 9) appears to contain a large periodic signal superimposed on the seasonal Fraser cycle. A power spectrum of the plume surface area (not shown), computed with the same spectral method and windowing parameters used to estimate the periodogram of plume salinity (Figure 6), shows that the spectral energy is primarily concentrated in the 8–15 day range. Thus there is little or at least ambiguous evidence of fortnightly cycling in the plume surface area, unlike salinity. The Fraser has little spectral energy in the 8–15 day band, and thus it is not likely causing the 8–15 day variance in plume area. Advection of the plume by wind relative to the ferry track may complicate the surface area time series. Estimates of plume area on weekly time scales or shorter would likely be affected.

[64] At the semidiurnal and diurnal scales, a Lomb-Scargle periodogram of track-by-track surface area reveals a noisy red spectrum. There are no significant cycles at any of the main tidal constituents. Intuitively, the plume surface area should be larger at low water because the river discharges more water than at high tide. However, it is likely that any significant cycle in area is buried in noise due to physical variability and sampling errors.

[65] Tidal effects are evident in the along-strait location of the plume. Advection by tides in the SoG are on the order of 10 km, so we would expect to see changes in the offshore extent of the plume by tidal advection. A Lomb-Scargle periodogram of the position of the offshore extent shows tidal lines, though they are somewhat weaker than those of plume salinity. At longer scales, a Welch PSD of daily averaged offshore extent shows broad ($\Delta t \approx 10$ days) energy peak at 15 days, and the effect appears stronger in summer.

## 6. Conclusion

[66] With a novel data set based on an instrumented ferry we have been able to identify how river discharge and tides set the near-field salinity of a river plume, and how river discharge sets the plume surface area. The temporal resolution is fine enough to resolve tidal effects in the diurnal and semidiurnal bands, and the length is of sufficient duration to identify seasonal changes.

[67] Plume salinity is a quasi-linear function of river discharge on time scales of 25 days or more, and ranges from 25 PSU at 1000 m$^3$ s$^{-1}$ to 15 PSU at 8000 m$^3$ s$^{-1}$. The plume contains more fresh water at high river discharge than low, but the fresh water residence time is roughly constant throughout the year.

[68] The tides operate on the plume salinity over three time scales, semidiurnal, diurnal, and fortnightly. The plume is fresher at lower-low water than higher-high water. The low-salinity water originates from the river as the discharge increases during the ebb cycle. On a single large ebb during the summer, the mean plume salinity can drop as much as 5 PSU. In winter during low river flows, the amplitude of tidal signal is reduced and changes of about 1 or 2 PSU at the end of a large ebb tide are common. On fortnightly scales, particularly during summer, the plume salinity fluctuates in phase with the daily maximum tidal height, being fresher during neap tides and saltier during spring tides by a few PSU. Both the ebb/flood and fortnightly tidal cycles are superimposed on the river flow seasonal cycle, and the magnitude of their effects increases with increasing river discharge.

[69] We were able to ground-truth estimates of surface area seen by the ferry with remote sensing data. Errors inherent in using the ferry to estimate surface area likely dominate natural high-frequency variations. On longer time scales, plume surface area is proportional to the river discharge at the mouth. On the basis of the low-pass filtered time series, the plume area ranges from 200–500 km$^2$ at low river flow to 1000–1500 km$^2$ during freshets. A linear fit to the discharge versus area yields an increase in 140 km$^2$ per 1000 m$^3$ s$^{-1}$. Rotation and buoyancy appear to govern the plume surface area according to the *Yankovsky and Chapman* [1997] surface advected plume formulation. Inertial effects appear to be irrelevant in the larger-scale plume structure because the high-outflow Froude number limit of (3) substantially underpredicts the surface area. Although the low-outflow Froude number limit of the *Yankovsky and Chapman* [1997] estimates the magnitude of the plume surface area well, it predicts a linear relationship, while there is a weak curvature in the data.

[70] The strong modulation of tidal effects by river flow on the plume salinity complicate the idea of categorizing the section of the plume sampled by the ferry as a near field. The enhanced tidal effects at high river flow suggest the ferry samples the near-field plume, while in winter it appears that the near-field plume remains much closer to the river mouth (or does not exist) because observed tidal

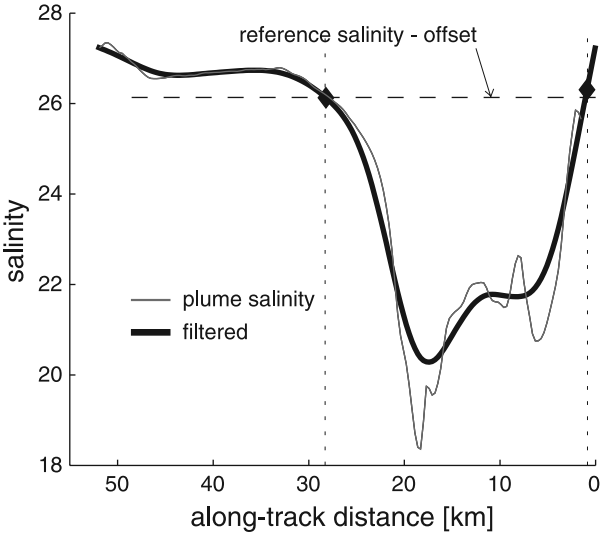


**Figure B1.** Shown is a typical salinity transect through the plume, taken during a time of moderate river discharge ($\sim$3000 $m^3$ $s^{-1}$). The thin gray line is the original data, and the heavy black line was filtered with a sliding boxcar 1/10th the width of the transect. The plume is defined as part of the transect having a salinity lower than $S_{ref} - S_{offset}$.

effects are weak. The changing character of the estuary and river plume with river flow resembles the results of *Garvine* [1975] in the Connecticut River Estuary where the sharpest salinity gradients move out of the estuary at high flows. Likewise we suggest that the dependence on river flow of the location of the salt wedge with respect to the river mouth causes the winter/summer differences in the Fraser Estuary and plume.

[71] The Fraser River near-field plume and estuary also appears to be a close relative of the Columbia in a few respects. First, the systems are very strongly forced; they share a similar tidal range, mouth width, and river discharge (though much of the seasonality of the Columbia has been diminished by dams). Both exhibit a low mouth Kelvin number, signifying the importance of momentum in defining the dynamics at the river mouth. Second, both systems exhibit a change in mixing at the salt wedge as a function of the fortnightly tidal cycle. The analogy between the systems likely ends in the far field of the river plume, where wind is the dominant external force. The Fraser lies within a nearly enclosed system while the Columbia discharges onto a shelf. This may affect the far-field dynamics in two respects. First, the Fraser plume may span the SoG and reach a lateral barrier. Second, the Ekman flows driven by wind are very important in coastal shelf systems, whereas wind driven circulation in the SoG will likely respond differently.

## Appendix A: Fraser Discharge at the Mouth

[72] Most references to the Fraser River flow refer to the volume discharge measured at the Water Survey of Canada's Hope, BC, gauge station (ID 08MF005). It lies 120 km upstream of the mouth and is the nearest active station to the mouth that does not experience tidal fluctuations. *Pawlowicz et al.* [2007] have shown that the discharge at the Port Mann bridge (08MH126), 35 km upstream of the mouth and downstream of all major tributaries, can exceed the Hope discharge by 20% in the summer and nearly 100% in the winter. These results were obtained from a linear regression between the weekly mean discharge at Hope and the discharge at Port Mann. However, for this study we require data which captures the river discharge on daily time scales.

[73] Discharge is not measured at Port Mann, though daily data from a model run by the Water Survey of Canada is available for limited times. Model output at Port Mann is not available for the years 2003–2006. To estimate the river discharge at Port Mann for the years 2003–2006, we developed a relationship between discharge at Port Mann and Hope from historical data and then apply the results to the Hope discharge from 2003 to 2006. To account for the contribution of ungauged small rivers, a regression was used to scale the Chehalis River (08MG001) to represent the sum of all the small drainage rivers and creeks that join the Fraser downstream of Hope (the Chehalis is a relatively small river with a gross drainage area of 383 $km^2$).

[74] The regression was performed between the flow at Port Mann minus the Fraser River at Hope minus the Harrison River and the Chehalis River (the Harrison River, 08MG013, is the largest tributary of the Fraser downstream of Hope). Thus, the flow at Port Mann would be represented by:

$$Q_{PortMann} = Q_{Hope} + Q_{Harrison} + a + bQ_{Chehalis} \qquad \text{(A1)}$$

where $Q$ represents volume discharge and $a$ and $b$ were determined by a least squares regression to be 112 and 7.71, respectively. A 10 year span, from 1983 to 1993, of daily discharge was used in the analysis. The Chehalis time series was lagged by 1 day, reducing the standard deviation of the residuals by 10% compared to the original fit. The result of the fit is a straight line with about 500 $m^3$ $s^{-1}$ of scatter, while only a small fraction points miss by a larger margin.

## Appendix B: Defining the Plume

[75] River plumes have several unique properties which distinguish them from ocean water, but salinity is the easiest to measure. A typical transect of salinity as a function of along-strait distance, taken during a time of moderate river discharge, is shown in Figure B1. The $x$ axis is reversed because 0 km lies near Tsawwassen, on the eastern side of the SoG, and 55 km is on the western side. In this example, and in the majority of transects, the plume is found in the southeastern half of the transect, and is apparent by the dip in salinity between 0 and 30 km. At greater along-strait distances (northwest of the plume, near Vancouver Island), the salinity is roughly constant.

[76] The plume is defined as the part of the transect which has a salinity $S < S_{ref} - S_{offset}$. The reference salinity is the spatial mean of salinity between 45 and 50 km, which lies outside the plume (see Figure 3). It is calculated for each individual transect. In some respects $S_{offset}$ is arbitrary, so we have decided to make it a linear function of the reference salinity. It varies between 0.4 to 1.8 PSU. It is highest during periods when the reference salinity is low, which corresponds to times when the difference between the plume salinity and reference salinity is highest. If the

salinity offset were too high during low-flow periods, then much of the plume will be missed because it has a relatively high salinity. The broken line in Figure B1 shows $S_{ref} - S_{offset}$ for that particular transect. The salinity is then low-pass filtered in along-strait distance by a running mean filter having 10% of the width of the transect. The plume boundary is then chosen as the point where $S_{ref} - S_{offset}$ intersects the filtered salinity curve.

[77] **Acknowledgments.** Funding for this work was provided by the National Sciences and Engineering Research Council under grant 246274. The crew and staff at B. C. Ferry Services, Inc., gave tireless help and support; they made this study possible. Much of the instrumentation design and maintenance was done by Randall Lee. We would like to thank Nick Komick at UViC for MODIS imagery. Ted Tedford, Roger Pieters, and Susan Allen contributed helpful discussion, while Jordan Dawe provided helpful feedback on this manuscript. Lynn Campo at Environment Canada provided preliminary 2006 river discharge data.

## References

Abood, K. (1974), Circulation in the Hudson Estuary, in *Hudson River Colloquium*, edited by O. Roels, *Ann. N. Y. Acad. Sci.*, *250*, 38–111.

Ages, A. (1979), The salinity intrusion in the Fraser River: Salinity, temperature, and current observations, 1976, 1977, *Pac. Mar. Sci. Rep., 79-14*, Inst. of Ocean Sci., Sidney, B. C., Canada.

Chant, R. J., S. M. Glenn, E. Hunter, J. Kohut, R. F. Chen, R. W. Houghton, J. Bosch, and O. Schofield (2008), Bulge Formation of a Buoyant River Outflow, *J. Geophys. Res.*, *113*, C01017, doi:10.1029/2007JC004100.

Chao, S.-Y. (1988), Wind-driven motion of estuarine plumes, *J. Phys. Oceanogr.*, *18*, 1144–1166.

Chatwin, P. (1976), Some remarks on the maintenance of the salinity distribution in estuaries, *Estuarine Coastal Mar. Sci.*, *4*, 555–566.

Cleveland, W. (1979), Robust locally weighted regression and smoothing scatterplots, *J. Am. Stat. Assoc.*, *74*, 829–836.

Cordes, R., S. Pond, B. de Lange Boom, and P. LeBlonde (1980), Estimates of entrainment in the Fraser River plume, British Columbia, *Atmos. Ocean*, *18*, 15–26.

Crean, P., T. Murty, and J. Stronach (1988), *Mathematical Modelling of Tides and Estuarine Circulation: The Coastal Seas of Southern British Columbia and Washington State, Lect. Notes on Coastal and Estuarine Stud.*, vol. 30, Springer, New York.

Fischer, H., E. List, R. Koh, J. Imberger, and N. Brooks (1979), *Mixing in Inland and Coastal Waters*, 1st ed., Academic, New York.

Fong, D., and W. Geyer (2002), The alongshore transport of freshwater in a surface-trapped river plume, *J. Phys. Oceanogr.*, *32*, 957–972, doi:10.1175/1520-0485(2002)032<0957:TATOFI>2.0.CO;2.

Foreman, M., R. Walters, R. Henry, C. Keller, and A. Dolling (1995), A tidal model for Juan-de-Fuca Strait and the Southern Strait of Georgia, *J. Geophys. Res.*, *100*(C1), 721–740, doi:10.1029/94JC02721.

Garvine, R. (1975), The distribution of salinity and temperature in the Connecticut River Estuary, *J. Geophys. Res.*, *80*(9), 1176–1183.

Garvine, R. (1987), Estuary plumes and fronts in shelf waters: A layer model, *J. Phys. Oceanogr.*, *17*, 1877–1896.

Geyer, W., and D. Farmer (1989), Tide-induced variation of the dynamics of a salt wedge estuary, *J. Phys. Oceanogr.*, *19*, 1060–1072.

Geyer, W., P. Hill, T. Milligan, and P. Traykovski (2000), The structure of the Eel River plume during floods, *Cont. Shelf Res.*, *20*, 2067–2093.

Hansen, D., and M. Rattray (1965), Gravitational circulation in straits and estuaries, *J. Mar. Res.*, *23*, 104–122.

Hetland, R. (2005), Relating river plume structure to vertical mixing, *J. Phys. Oceanogr.*, *35*(9), 1667–1688.

Hetland, R., and W. Geyer (2004), An idealized study of the structure of long, partially mixed estuaries, *J. Phys. Oceanogr.*, *34*(12), 2677–2691.

Hickey, B., L. Pietrafesa, D. Jay, and W. Boicourt (1998), The Columbia River plume study: Subtidal variability in the velocity and salinity fields, *J. Geophys. Res.*, *103*(C5), 10,339–10,368, doi:10.1029/94JC00343.

Hodgins, D., J. S. Hardy, and S. E. Tinis (1994), Remote sensing of surface currents in the Fraser River plume with the SeaSonde HF radar, *Rep. EE-151*, Emergencies Sci. Div., Environ. Technol. Cent., Environ. Can., Ottawa, Ont., Canada.

Jay, D., and J. Smith (1990), Circulation, density distribution and neap-spring transitions in the Columbia River Estuary, *Prog. Oceanogr.*, *25*, 81–112.

Kirk, J. (1994), *Light and Photosynthesis in Aquatic Ecosystems*, 2nd ed., Cambridge Univ. Press, New York.

Kostaschuk, R., and L. Atwood (1990), River discharge and tidal controls on salt-wedge position and implications for channel shoaling: Fraser River, British Columbia, *Can. J. Civil Eng.*, *17*(3), 452–459.

Kranenburg, C. (1986), A time scale for long-term salt intrusion in well-mixed estuaries, *J. Phys. Oceanogr.*, *16*, 1329–1331.

Lentz, S. (1995a), The Amazon River plume during AMASSEDS: Subtidal current variability and the importance of wind forcing, *J. Geophys. Res.*, *100*(C2), 2377–2390, doi:10.1029/94JC00343.

Lentz, S. (1995b), Seasonal variations in the horizontal structure of the Amazon Plume inferred from historical hydrographic data, *J. Geophys. Res.*, *100*(C2), 2391–2400, doi:10.1029/94JC01847.

Li, R., Y. Kaufman, B. Gao, and C. Davis (2003), Remote sensing of suspended sediments and shallow coastal waters, *IEEE Trans. Geosci. Remote Sens.*, *41*(3), 559–566.

Lomb, N. (1976), Least-squares frequency analysis of unequally spaced data, *Astrophys. Space Sci.*, *39*(2), 447–462.

MacCready, P. (2007), Estuarine adjustment, *J. Phys. Oceanogr.*, *37*(8), 2133–2145.

MacCready, P., R. Hetland, and W. Geyer (2002), Long-term ishaline salt balance in an estuary, *Cont. Shelf Res.*, *22*, 1591–1601.

MacDonald, D. (2003), Mixing processes and hydraulic control in a highly stratified estuary, Ph.D. thesis, Mass. Inst. of Technol., Cambridge.

MacDonald, D., and W. Geyer (2004), Turbulent energy production and entrainment at a highly stratified estuarine front, *J. Geophys. Res.*, *109*, C05004, doi:10.1029/2003JC002094.

MacDonald, D., L. Goodman, and R. Hetland (2007), Turbulent dissipation in a near-field river plume: A comparison of control volume and microstructure observations with a numerical model, *J. Geophys. Res.*, *112*, C07026, doi:10.1029/2006JC004075.

Melchior, P. (1966), *The Earth Tides*, Pergamon, Oxford, U. K.

Monismith, S., W. Kimmerer, J. Burau, and M. Stacey (2002), Structure and flow-induced variability of the subtidal salinity field in northern San Francisco Bay, *J. Phys. Oceanogr.*, *32*, 3003–3019.

Partch, E., and J. Smith (1978), Time dependent mixing in a salt wedge estuary, *Estuarine Coastal Mar. Sci.*, *6*, 3–19.

Pawlowicz, R. (2002), Classical tidal harmonic analysis including error estimates in MATLAB using T_TIDE, *Comput. Geosci.*, *28*, 929–937.

Pawlowicz, R., O. Riche, and M. Halverson (2007), The circulation and residence time of the Strait of Georgia using a simple mixing-box approach, *Atmos. Ocean*, *45*(4), 173–193, doi:10.3137/ao.450401.

Percival, D., and A. Walden (1993), *Spectral Analysis for Physical Applications: Multitaper and Conventional Univariate Techniques*, Cambridge Univ. Press, New York.

Peters, H. (1997), Observations of stratified turbulent mixing in an estuary: Neap-to-spring variations during high river flow, *Estuarine Coastal Shelf Sci.*, *45*, 69–88.

Royer, L., and W. Emery (1982), Variations of the Fraser River plume and their relationship to forcing by tide, wind and discharge, *Atmos. Ocean*, *20*, 357–372.

Scargle, J. (1982), Studies in astronomical time series analysis. II. Statistical aspects of spectral analysis of unevenly spaced data, *Astrophys. J.*, *263*, 835–853.

Stronach, J. (1981), The Fraser River plume, Strait of Georgia, in *Ocean Management*, vol. 6, pp. 201–221, Elsevier, New York.

Tabata, S. (1972), The movement of the Fraser River-influenced water in the Strait of Georgia as deduced from a series of aerial photographs, *Pac. Mar. Sci. Rep., 72-6*, 69 pp., Mar. Sci. Branch, Pac. Reg., Victoria, B. C., Canada.

Thomas, A., and R. Weatherbee (2006), Satellite-measured temporal variability of the Columbia River plume, *Remote Sens. Environ.*, *100*, 167–178.

Waldichuk, M. (1957), Physical oceanography of the Strait of Georgia, British Columbia, *J. Fish. Res. Board Can.*, *14*, 321–486.

Warrick, J., and D. Fong (2004), Dispersal scaling from the world's rivers, *Geophys. Res. Lett.*, *31*, L04301, doi:10.1029/2003GL019114.

Yankovsky, A., and D. Chapman (1997), A simple theory for the fate of buoyant coastal discharges, *J. Phys. Oceanogr.*, *27*, 1386–1401.

M. J. Halverson and R. Pawlowicz, Department of Earth and Ocean Sciences, University of British Columbia, 6339 Stores Road, Vancouver, BC V6T 1Z4, Canada. (mhalverson@eos.ubc.ca)